Article

progress in Reaction Kinetics and Mechanism

Progress in Reaction Kinetics and Mechanism
Volume 45: 1–17

DOI: 10.1177/1468678320901622
journals.sagepub.com/home/prk
SAGE

Methane–propane hydrate formation and memory effect study with a reaction kinetics model

Wei Ke[1,2], Guang-Jin Chen[3] and Daoyi Chen[1]

Abstract

Although natural gas hydrates and hydrate exploration have been extensively studied for decades, the reaction kinetics and nucleation mechanism of hydrate formation is not fully understood. In its early stage, gas hydrate formation can be assumed to be an autocatalytic kinetic reaction with nucleation and initial growth. In this work, a reaction kinetics model has been established to form structure II methane–propane hydrate in an isochoric reactor. The computational model consists of six pseudo-elementary reactions for three dynamic processes: (1) gas dissolution into the bulk liquid, (2) a slow buildup of hydrate precursors for nucleation onset, and (3) rapid and autocatalytic hydrate growth after onset. The model was programmed using FORTRAN, with initiating parameters and rate constants that were derived or obtained from data fitted using experimental results. The simulations indicate that the length of nucleation induction is determined largely by an accumulation of oligomeric hydrate precursors up to a threshold value. The slow accumulation of precursors is the rate-limiting step for the overall hydrate formation, and its conversion into hydrate particles is critical for the rapid, autocatalytic reaction. By applying this model, the memory effect for hydrate nucleation was studied by assigning varied initial amounts of precursor or hydrate species in the simulations. The presence of pre-existing precursors or hydrate particles could facilitate the nucleation stage with a reduced induction time, and without affecting hydrate growth. The computational model with the performed simulations provides insight into the reaction kinetics and nucleation mechanism of hydrate formation.

[1]Division of Ocean Science and Technology, Graduate School at Shenzhen, Tsinghua University, Shenzhen, P. R. China
[2]Department of Petroleum Engineering, Faculty of Science and Technology, University of Stavanger, Stavanger, Norway
[3]State Key Laboratory of Heavy Oil Processing, China University of Petroleum, Beijing, P. R. China

Corresponding authors:
Guang-Jin Chen, State Key Laboratory of Heavy Oil Processing, China University of Petroleum, Beijing 102249, P. R. China.
Email: gjchen@cup.edu.cn

Daoyi Chen, Division of Ocean Science and Technology, Graduate School at Shenzhen, Tsinghua University, Shenzhen 518055, Guangdong, P. R. China.
Email: Chen.daoyi@sz.tsinghua.edu.cn

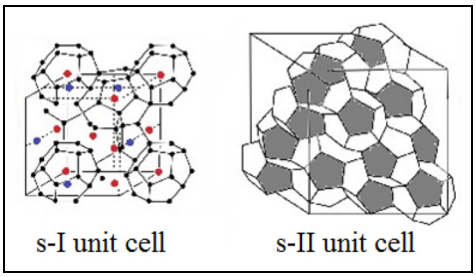

Figure 1. Unit cell assembly of crystalline structure I (s-I) and structure II (s-II) gas hydrates. The s-I unit cell consists of 2 small 512 cavities and 6 large 51262 cavities, and the s-II unit cell consists of 16 small 512 cavities and 8 large 51264 cavities.
Source: Figure adapted from Steed and Atwood.[3]

Keywords
Gas hydrates, reaction kinetics, modeling, autocatalysis, memory effect

Introduction

Gas hydrates are crystalline structures that are formed from water and gas at high pressures and low temperatures.[1] Typical "guest" molecules, such as methane, ethane, propane, and carbon dioxide, are entrapped in "host" water cages, which mostly yield cubic crystals of structure I (s-I) or structure II (s-II)[2] with microscopic constructions of s-I and s-II hydrate unit cells as illustrated in Figure 1.***

Gas hydrates are an industry nuisance when they form in oil–gas pipelines and prevent flow, which causes flow-assurance issues.[4] Common circumstances include that the residual water in the multiphase flow or on the pipe wall would react with suitable natural gas components both above the liquid phase and inside the bulk fluid to form hydrate particles. The process can be slow initially and catastrophic eventually, producing a large amount of hydrate accumulated along the pipe wall and inside the bulk, very likely in the form of a hydrate plug. Remediation of formed hydrate plug to remove the blocking of oil and gas flow usually costs a great deal and causes inconvenience to the production practices by oil companies. On the other hand, the enormous amount of in situ methane hydrates that exist in permafrost and oceanic sediments offers high potential as a future clean-energy source.[5,6] It has been debated whether exploration or the in situ melting of hydrates would damage the climate and environment severely, should an unexpected release of methane gas occur.[7,8] Recently, researchers have started to study hydrates for use in rewarding engineering applications, such as carbon capture and storage,[9,10] hydrate-based gas separation,[11] hydrogen storage,[12] and seawater desalination.[13]

From a hydrate-science perspective, the knowledge gap is that its nucleation mechanism is not understood fully, nor has the overall formation process been described in detail. Hydrate formation is divided empirically into two consecutive stages of nucleation and growth with no rigid boundary between them. The rapid, catastrophic growth stage is controlled mainly by mass transfer,[14–17] heat transfer,[18–21] or coupled mechanisms[22–28] that include intrinsic

kinetics.[29–33] Primary nucleation is a free-energy-driven and statistically random process that is highly sensitive to the driving force. During nucleation and early-stage growth, the mass- and heat-transfer resistance is relatively small, with observable hydrate crystals not yet present in solution. In such cases, the intrinsic kinetics would be influential and should be considered. However, limited literature exists on applying reaction kinetics methodologies (e.g. enzymatic and autocatalytic reactions[34]) with numerical computations to study hydrate formation. This could be because there is no chemical bonding or strong force between the host and guest molecules in gas-hydrate structures. Weak van der Waals forces maintain the hydrate crystalline structure stability.[35]

The aims of this study were to develop a computational model for s-II methane–propane hydrate formation and obtain insights into its intrinsic reaction kinetics and molecular mechanism via numerical simulations. The modeling involved challenging tasks to derive reasonable pseudo-elementary reactions, corresponding rate equations, model computation, and deduction of rate constants. The model was used to simulate several key steps in the hydrate-formation process. These included gas dissolution, a slow accumulation of hydrate precursors, slow hydrate formation, and rapid autocatalytic hydrate growth. The simulation results for the fresh water–gas system were compared with experimental hydrate data so one could see to what extent the model could simulate the process. The so-called "memory effect" phenomenon, which indicates that hydrate onset occurs more rapidly and less randomly if the aqueous phase involves a thermal history of a previous hydrate or ice formation and melting process,[29,36,37] was also studied with the model. A current hypothesis is that a trace amount of residual clusters of water molecules or hydrate-cage-like structures remain in the aqueous phase after hydrate dissociation and before the next-round hydrate formation. Positive and negative results that support and oppose this hypothesis, respectively, have both been reported from experimental studies,[38,39] and molecular dynamics (MD) simulations.[40–42] The methodology to establish a reaction kinetics–based computational model for simulations could provide an alternative approach to study hydrate-formation kinetics and may yield new insights into the process. Such an understanding is important to both hydrate science and engineering.

Experimental

Experimental setup

Figure 2 shows a schematic diagram of the isochoric experimental apparatus and setup. A high-pressure titanium autoclave was used as the hydrate-formation vessel. The reactor with a cylindrical geometry had an inner volume of 141.3 mL. The temperature was measured using a 1/10 DIN Pt-100 temperature sensor with an overall accuracy of ± 0.1 K. Two temperature sensors were mounted to allow for simultaneous temperature monitoring in the vapor and aqueous phases. A pressure gauge with a Rosemount 3051 TA absolute pressure transmitter provided pressure readings with an accuracy of ± 0.02 MPa. A refrigerating and heating circulator (model Julabo F 34 HL) was used for temperature control by circulating cooling/heating water through the water jacket of the reactor. It had an integrated programmable user interface with a temperature stability of ± 0.01 K. LabView was installed on the laboratory personal computer to monitor and record data at 3-s intervals to show real-time pressure/temperature (PT) variations on the computer screen.

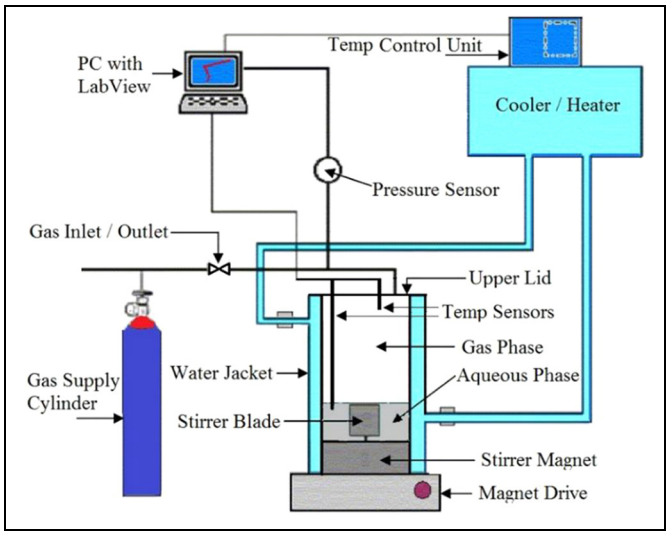

Figure 2. Experimental apparatus and setup used in gas-hydrate studies.

The gas cylinder delivered a synthesized natural gas mixture (SNG2) of methane and propane supplied by Praxair Norway, of 92.5 mol% methane and 7.5 mol% propane. SNG2 gas and water form s-II hydrate. The binary SNG2 has the same composition, thermodynamic properties, and equilibrium curve as that investigated by Abay and Svartaas.[43]

Experimental method

To obtain realistic rate constants for the modeling and simulation, gas-dissolution tests were performed prior to the hydrate-formation experiments. Gas dissolution and hydrate-formation experiments were conducted under isochoric and isothermal conditions. The preparation stage for each experiment was similar. The reactor was cleaned thoroughly, rinsed with distilled water, and air-dried. Before changing the vapor phase to the experimental PT conditions, the reactor was purged twice with the actual gas at 4.0 MPa to remove residual air.

Gas-dissolution tests were carried out with 91.3-mL SNG2 gas and 50-mL distilled water at 6.3 MPa and 293.15 K. Agitation (750 r/min) was used to stir the gas into the aqueous phase. The amount of free SNG2 gas in the reactor, initially, during, and after the dissolution process was calculated using the ideal gas equation $PV = znRT$. The compressibility factor, z, was calculated based on the Dranchuk and Abou–Kassem equation of state.

In the hydrate-formation experiments, 91.3-mL SNG2 gas and 50-mL distilled water were loaded into the reactor and stabilized at 6.3 MPa and 293.15 K. The system was cooled with a constant cooling rate of 2 K h^{-1} without stirring until it reached the experimental PT of 6.1 MPa and 288.15 K. The magnetic stirrer was started at a fixed rate of 750 r/min, which denoted the start of the experiment and time zero for the measurement of induction time. The induction time was measured from the start of stirring to the first sign that indicated hydrate onset, that is, the first temperature peak with gas consumption (Figure 3).

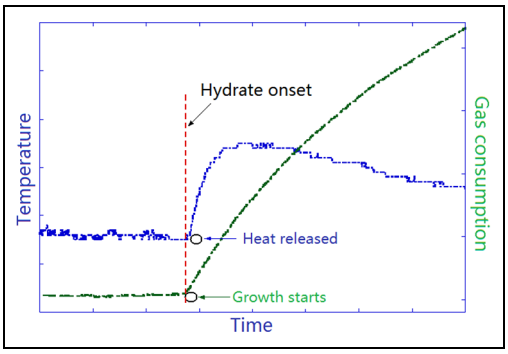

Figure 3. Illustration of temperature (left Y-axis, blue curve) and gas consumption (right Y-axis, green curve) variations shortly before and after hydrate onset.

Computational model

The reaction kinetics model proposed for s-II methane–propane hydrate formation and the simulation process are described below. The following two assumptions were considered:

1. The nucleation and initial growth stage with no observable hydrate crystals is controlled mainly by the intrinsic reaction kinetics. In a water-access system, the mass-transfer resistance is reflected partially by integrating gas dissolution in the model.
2. The three-phase mixture that contains water, gas, and hydrate/precursors is assumed to be a homogeneous slurry that bears uniform physical and thermodynamic properties.

The following sections present the pseudo-elementary kinetic reactions, the rate equations, the computing process, and the deduction of rate constants for the simulations, respectively.

Pseudo-elementary kinetic reactions

Our computational model comprised six pseudo-elementary reactions, which were defined by processes $M1$–$M5$ (see graphical illustration in Figure 4). Seven time-dependent variables, including three reactants and four products, were involved in this specific hydrate-forming system. The reactants were water (H_2O), and free gas components methane (CH_4(g)) and propane (C_3H_8(g)). The products were hydrate particles (**H**), and three reaction intermediates, that is, dissolved methane (CH_4(aq)), dissolved propane (C_3H_8(aq)), and hydrate precursors (**N**), where **N** refers to incomplete hydrate-cage-like structures.

As illustrated in Figure 4, $M1a$ and $M1b$ describe the dissolution and effervescence processes of gaseous methane and propane into and out of the liquid phase. $M2$ describes the reversible formation of precursors **N** from dissolved gas and water. $M3$ is a slow, uncatalyzed formation of methane–propane hydrate **H** from species **N**. $M4$ and $M5$ are two autocatalytic reactions that describe the formation of **H** from precursors **N** and from the dissolved gas and water, respectively. CH_4(g) and C_3H_8(g) in $M1a$ and $M1b$ share the same rate constants k_1 and k_{-1} for their dissolution kinetics. This simplification is supported by the flash

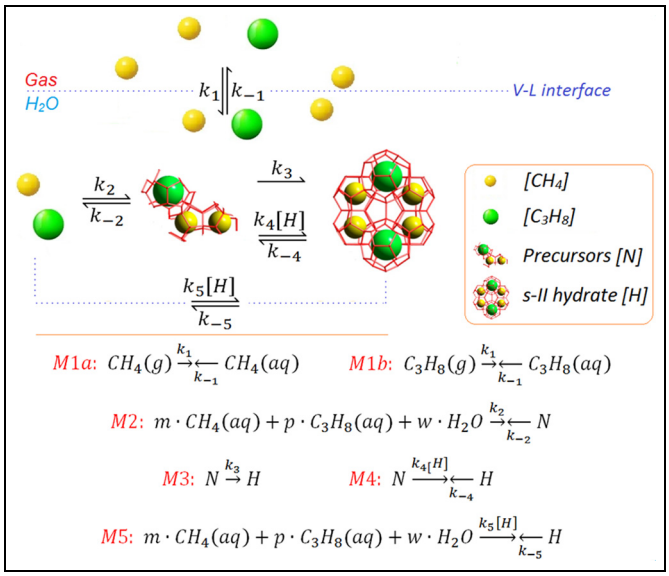

Figure 4. A reaction kinetics model with pseudo-elementary processes established for s-II methane–propane hydrate formation.

calculations of molar composition of hydrate–water–gas phases in previous work using SNG2 gas by Abay and Svartaas.[43]

Rate equations

With defined pseudo-elementary processes M1–M5 described in the "Pseudo-elementary kinetic reactions" section, rate equations for each reactant and product can be written as equations (1)–(7) below and solved mathematically. The use of square brackets refers to the real-time mass (in mol) of each component in the system. For example, [CH_4(aq)] is the mass of dissolved methane gas in the aqueous phase in mol, a time-dependent variable along the entire reaction/simulation process. Variables m, p, and w are dimensionless, non-stoichiometric ratios for dissolved methane, propane, and water to react and form precursors **N** or hydrate particles **H** (M2 and M5). Mass variations in mol min^{-1} of the individual components are depicted as functions of time, rate constants, and varying mass of involved species

$$\frac{d[\mathrm{CH_4(g)}]}{dt} = -k_1[\mathrm{CH_4(g)}] + k_{-1}[\mathrm{CH_4(aq)}] \tag{1}$$

$$\begin{aligned}\frac{d[\mathrm{CH_4(aq)}]}{dt} &= k_1[\mathrm{CH_4(g)}] - k_{-1}[\mathrm{CH_4(aq)}] \\ &\quad + m(k_{-2}[\mathbf{N}] + k_{-5}[\mathbf{H}] - (k_2 + k_5[\mathbf{H}])[\mathrm{CH_4(aq)}]^m[\mathrm{C_3H_8(aq)}]^p[\mathrm{H_2O}]^w)\end{aligned} \tag{2}$$

$$\frac{d[\mathrm{C_3H_8(g)}]}{dt} = -k_1[\mathrm{C_3H_8(g)}] + k_{-1}[\mathrm{C_3H_8(aq)}] \tag{3}$$

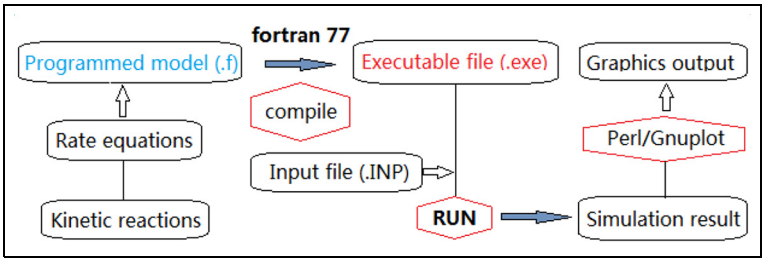

Figure 5. Simulation and computing flow chart.

$$\frac{d[C_3H_8(aq)]}{dt} = k_1[C_3H_8(g)] - k_{-1}[C_3H_8(aq)] + p(k_{-2}[\mathbf{N}] + k_{-5}[\mathbf{H}] - (k_2 + k_5[\mathbf{H}])[CH_4(aq)]^m[C_3H_8(aq)]^p[H_2O]^w) \quad (4)$$

$$\frac{d[H_2O]}{dt} = w(k_{-2}[\mathbf{N}] + k_{-5}[\mathbf{H}] - (k_2 + k_5[\mathbf{H}])[CH_4(aq)]^m[C_3H_8(aq)]^p[H_2O]^w) \quad (5)$$

$$\frac{d[N]}{dt} = k_2[CH_4(aq)]^m[C_3H_8(aq)]^p[H_2O]^w - (k_{-2} + k_3)[\mathbf{N}] + (k_{-4} - k_4[\mathbf{N}])[\mathbf{H}] \quad (6)$$

$$\frac{d[\mathbf{H}]}{dt} = k_5[\mathbf{H}][CH_4(aq)]^m[C_3H_8(aq)]^p[H_2O]^w + (k_3 + k_4[\mathbf{H}])[\mathbf{N}] - (k_{-4} + k_{-5})[\mathbf{H}] \quad (7)$$

Model computations

FORTRAN was used to program the established reaction kinetics model with the derived rate equations. The fortran77 compiler version was used for compiling and generating executable (.exe) files for numerical computations. The rate equations (1)–(7) were integrated with FORTRAN subroutine LSODE.[44] Double-precision computations were performed on a UNIX system at the University of Stavanger, and on a LINUX system using the Ubuntu platform (version 14.04 LTS) at Tsinghua University. Figure 5 shows a flowchart of the simulation and computing process.

A user-defined input (INP) file was called each time for input values to run the executable file. In the INP file, the following parameters were specified: (1) the initial amounts of species at $t = 0$, (2) the rate constants and non-stoichiometric factors, and (3) the simulation time and time step. In a fresh system with 91.3-mL SNG2 and 50-mL water, the initial amounts were $[CH_4(g)] = 0.247$ mol, $C_3H_8(g) = 0.020$ mol, and $[H_2O] = 2.780$ mol. A time step of 0.1 min was used. GNUPLOT, as integrated in PERL, generated graphical output with the computed numerical results.

Deduction of rate constants and factors

The deduction of k_1 and k_{-1} in processes $M1a$ and $M1b$ through gas-dissolution tests is presented in the "Experimental results" section. The other rate constants, k_2–k_{-5} in processes $M2$–$M5$, were data that were fitted subsequently with an induction time of 199.9 min, which was comparable with the 195.2 min that was measured during the experiment.

Table 1. Rate constants and non-stoichiometric factors used in numerical computations.

$k_1 = 1.13\times10^{-2}\text{min}^{-1}$		$k_{-1} = 3.20\text{min}^{-1}$
$k_2 = 1.64\times10^{-6}\text{M}^{1-m-p-w}\text{min}^{-1}$		$k_{-2} = 4.42\times10^{-3}\text{min}^{-1}$
$k_3 = 8.85\times10^{-3}\text{min}^{-1}$		
$k_4 = 9.71\times10^{10}\text{M}^{-1}\text{min}^{-1}$		$k_{-4} = 1.26\times10^{7}\text{min}^{-1}$
$k_5 = 7.58\times10^{6}\text{M}^{-m-p-w}\text{min}^{-1}$		$k_{-5} = 4.05\times10^{5}\text{min}^{-1}$
$m = 0.62$	$p = 0.38$	$w = 6.67$

Variables m, p, and w are dimensionless, nonstoichiometric ratios for dissolved methane, propane, and water to react and form precursors N or hydrate particles H (M_2 and M_5).

The non-stoichiometric factors, m, p, and w, are normalized values based on previous flash calculations by Abay and Svartaas.[43] Their calculation showed that the molar ratios of methane, propane, and water in the formed SNG2 hydrate phase were 0.0810, 0.0494, and 0.8696, respectively. The rate constants and factors used for numerical computations are summarized in Table 1.

Experimental results

SNG2 gas dissolution

The SNG2 gas-dissolution results are presented in Figure 6. No hydrate was formed as the dissolution experiment was conducted outside the hydrate region. The amount of dissolved gas (0.003 mol) was considerably less than that of free water (2.780 mol). Therefore, the dissolution process was expected to follow the standard reversible pseudo first-order kinetics[31] with the following rate law

$$\log\left(\frac{[\text{SNG2}]^{t}(\text{g}) - [\text{SNG2}]^{\infty}(\text{g})}{[\text{SNG2}]^{0}(\text{g}) - [\text{SNG2}]^{\infty}(\text{g})}\right) = -(k_1 + k_{-1})t \tag{8}$$

where $[\text{SNG2}]^{0}(\text{g})$ is the molar SNG2 concentration in the gas phase at time zero (prior to the start of stirring), $[\text{SNG2}]^{t}(\text{g})$ is the molar SNG2 concentration in the gas phase at time t, and $[\text{SNG2}]^{\infty}(\text{g})$ is the respective equilibrium value (liquid phase being saturated with SNG2 under stirring). The experimental gas-dissolution data are given in the Supplemental Material.

The rate constant k_1 was found through the slope in Figure 6(a) from the start of stirring. Figure 6(b) shows that the reversible pseudo first-order kinetics in equation (8) were obeyed, and a slope that equals $-(k_1 + k_{-1})$ resulted. The rate constants for SNG2 dissolution and effervescence into and out of the liquid phase were deduced as $k_1 = 1.13 \times 10^{-2}\ \text{min}^{-1}$ and $k_{-1} = 3.20\ \text{min}^{-1}$, respectively.

The k_1 and k_{-1} values that are derived here are valid for this experimental system only, with the specified setup, gas compositions, and the initial water–gas ratio. With a changed experimental setup or initial conditions, dissolution tests may have to be repeated and k_1 and k_{-1} re-determined for appropriate numerical computations.

Reaction of SNG2 with water

Figure 7 presents hydrate-formation data with PT profiles and mass variations of free SNG2 gas during the reactive phase. An abrupt pressure drop and a temperature peak upon onset

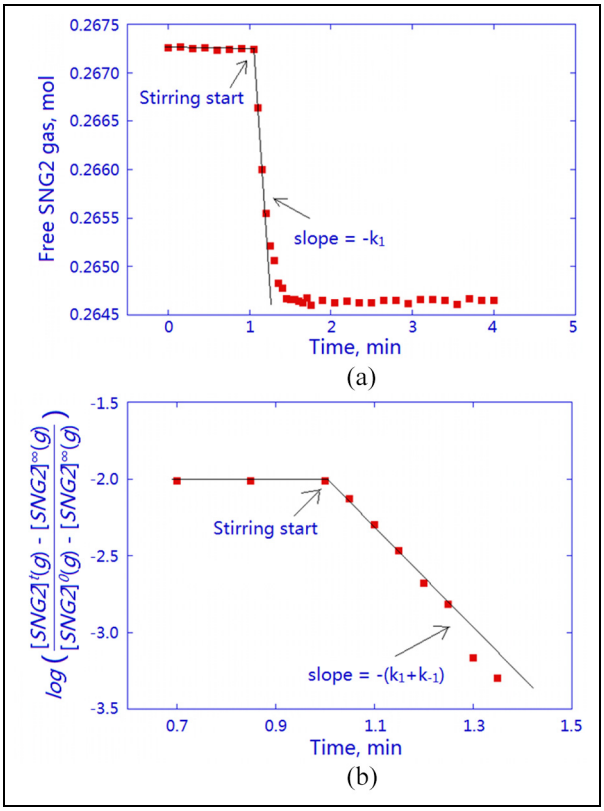

Figure 6. (a) Kinetics of the molar free SNG2 variations when the gas was stirred into the aqueous phase. Initial conditions: 6.3 MPa, 293.15 K, 50-g water (2.780 mol), 91.3-mL SNG2 (0.267 mol). (b) Plot showing that unreactive gas dissolution follows reversible first-order kinetics.

marked the beginning of the reactive phase, where SNG2 gas and water reacted with each other to form hydrates. The measured induction time was 195.2 min, followed by a growth period of 48 min before the reactor was heated and the hydrate-free region was re-entered.

A total of 2.298×10^{-2} mol of gas was consumed for hydrate conversion during the growth stage. The experimental hydrate nucleation and growth data are presented and compared with the simulation results in the following section. The measured SNG2 hydrate-formation data are given in the Supplemental Material.

Computational results

Clean water–gas system

Figure 8 shows the simulation results of hydrate nucleation and growth for a fresh SNG2–water system. Mass variations of free gases, CH_4(g) and C_3H_8(g), dissolved gases, CH_4(aq) and C_3H_8(aq), precursors **N**, and hydrate particles **H** were plotted against the simulation time.

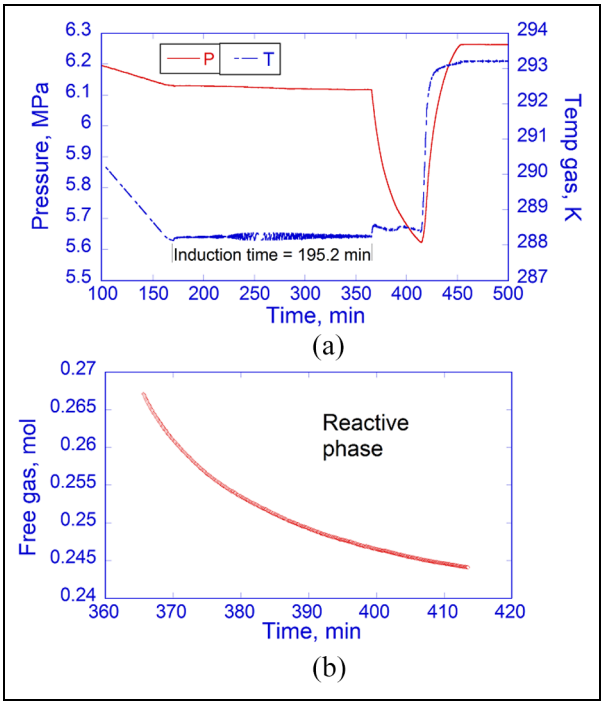

Figure 7. (a) PT profiles before and after hydrate onset in the hydrate formation experiment. The measured induction period was 195.2 min. (b) Growth period of 48 min (365–413 min) with SNG2 gas consumption in the reactive phase.
PT: pressure/temperature.

A small amount of water (0.152 mol, or 5.47 wt%) was consumed according to the simulation; therefore, its variation in this water-access system is not shown in Figure 8. The amount of formed hydrates was limited by the amount of free gas available. Both CH_4(aq) and C_3H_8(aq) were consumed instantly upon hydrate onset, followed by a mass reduction of CH_4(g) and C_3H_8(g) along the growth stage to accumulate hydrate mass **H**. The more apparent consumption of C_3H_8(aq) and C_3H_8(g) resulted from their much smaller amounts compared with those of CH_4(aq) and CH_4(g). After hydrate onset, a continuous gas supply from free gas dissolution ensured that the amounts of CH_4(aq) and C_3H_8(aq) were maintained at a relatively constant level. The amount of **N** accumulated gradually during the nucleation, reached a threshold value of 1.298×10^{-4} mol upon hydrate onset, and was kept constant thereafter. Therefore, CH_4(g) and C_3H_8(g) that were consumed after the nucleation contributed to the formation of **H** rather than **N**. Figure 9 compares the experimental and simulated results of the amount of formed hydrate and the growth rate after the nucleation stage.

It can be seen that the initial hydrate growth rate (during the first minute after onset) was 1.70×10^{-3} mol min^{-1} by experiment, while the simulated initial rate was merely 5.67×10^{-4} mol min^{-1}. The agreement on initial growth rate was non-ideal, indicating that the developed simulation package in its current form needs to be fine-tuned for more delicate computations.

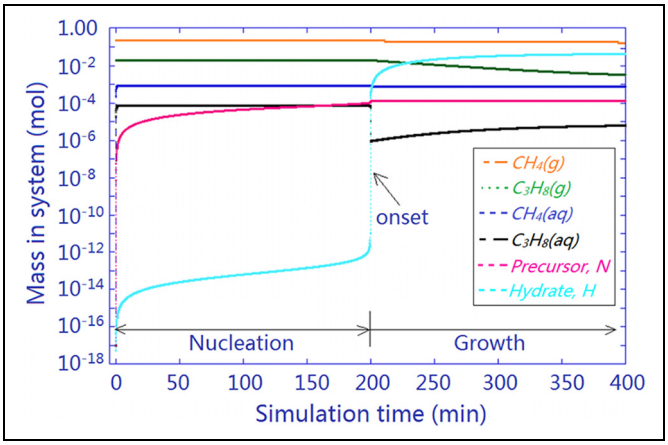

Figure 8. Simulated hydrate formation in a clean water–gas system with an induction period of 199.9 min and a growth stage thereafter. Initial conditions: 2.780-mol water, 0.247-mol methane, and 0.020-mol propane. Simulation time step: 0.1 min.

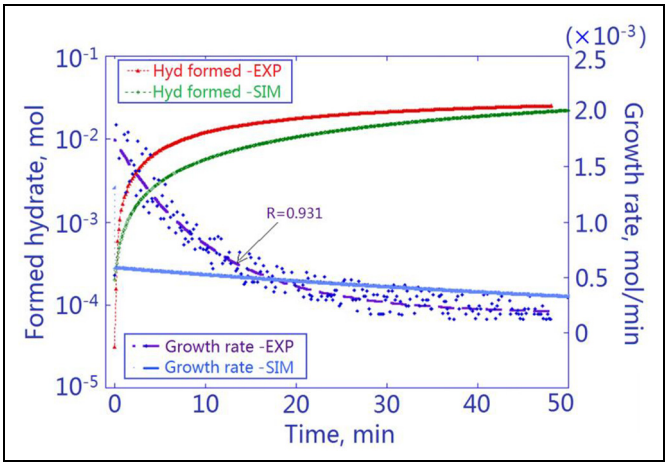

Figure 9. SNG2 hydrate formation: experimental versus simulation results. The blue dots are the real-time growth rates in the hydrate experiment, curve-fitted to give a decaying rate profile.

Subsequently, the experimental growth rate underwent a faster decay toward zero. The simulated hydrate formation, on the other hand, produced a milder growth profile with a slower hydrate accumulation and a slower decay in the rate of growth. Nevertheless, close average growth rates by experiment (4.79×10^{-4} mol min^{-1}) and simulation (4.55×10^{-4} mol min^{-1}) were observed. This led to a fair agreement on the total amount of hydrate formed (2.298×10^{-2} mol by experiment vs 2.275×10^{-2} mol by simulation) within the growth period.

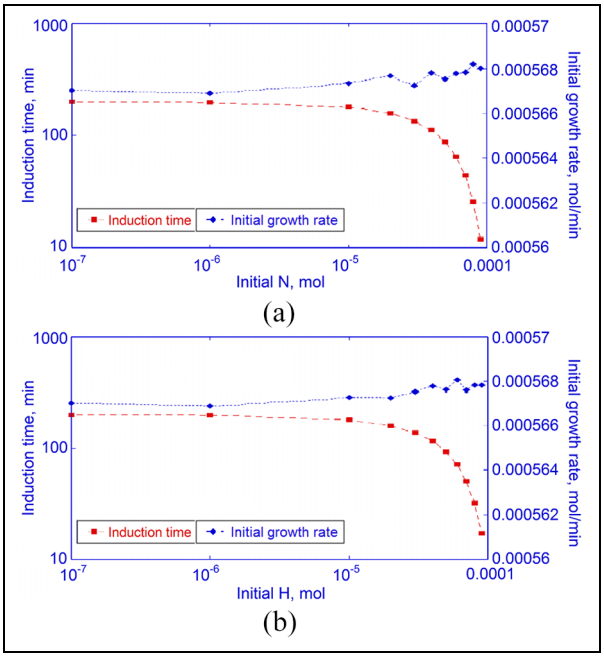

Figure 10. Impact of pre-existing (a) precursors **N** or (b) hydrate particles **H** on the length of nucleation induction and initial hydrate growth rate.

Pre-existing precursors/hydrates and memory effect

Varied initial amounts of **N** or **H** were assigned as inputs for the numerical computations. The computations mimic circumstances in which a very small fraction of **N** or **H** are not dissociated completely, or are seeded purposely[45] into the system prior to hydrate formation. If and how pre-existing **N** or **H** could facilitate hydrate formation was examined.

Figure 10 shows the effects of varied initial **N** or **H** from 1×10^{-7} to 9×10^{-5} mol on the length of nucleation induction and the initial growth rate (within the first minute after the simulated onset).

With pre-existing **N** or **H** increasing from 1×10^{-7} to 1×10^{-5} mol, the simulated induction time remained at nearly 200 min, which is approximately the same as in fresh water–gas systems. When pre-existing **N** or **H** increased from 1×10^{-5} to 9×10^{-5} mol, the induction time decreased significantly. The induction time was shortened to 11.9 min in the presence of 9×10^{-5} mol initial **N** (Figure 10(a)), or 18.7 min in the presence of 9×10^{-5} mol initial **H** (Figure 10(b)). The initial growth rate underwent a somewhat oscillating yet negligible increase from 5.67×10^{-4} to 5.68×10^{-4} mol min^{-1}, with varied initial **N** or **H**. Indeed, the simulated growth profile in the presence of initial **N** or **H** was found to be identical to that in fresh water–gas systems. The results suggest that pre-existing **N** or **H** has a major impact on the nucleation stage by effectively reducing the induction time, without affecting the growth stage. This is consistent with previous studies that the water history would affect the induction of nuclei emergence instead of the growth kinetics.[29]

Another point of interest with pre-existing **N** or **H** is whether it may affect the amount of **N** or **H** required to trigger the hydrate onset. Figure 11 presents simulation results showing

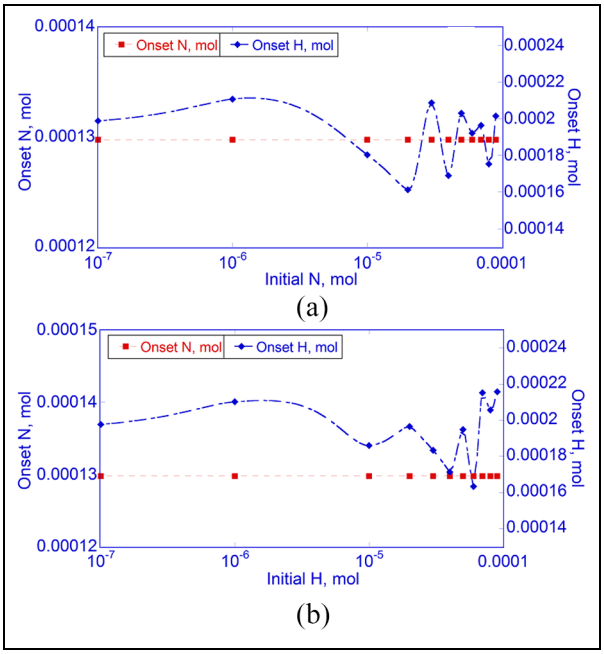

Figure 11. Effects of pre-existing (a) **N** or (b) **H** on the amount of precursors or hydrate particles upon hydrate onset. A constant threshold value of **N** at 1.298×10^{-4} mol (red, straight line) and an oscillating **H** with minor variations (interpolated, blue curve) were reported.

the amount of **N** or **H** upon hydrate onset as the initial **N** or **H** increased from 1×10^{-7} to 9×10^{-5} mol.

As the initial **N** varied from 1×10^{-7} to 9×10^{-5} mol, the amount of **H** at the onset point oscillated in the range $(1.6–2.2) \times 10^{-4}$ mol (Figure 11(a)). In contrast, the same rigid threshold value of **N** exists upon hydrate onset at 1.298×10^{-4} mol, as simulated in clean water–gas systems. Similarly, with a varied initial **H** from 1×10^{-7} to 9×10^{-5} mol, the amount of **H** at onset oscillated in the same range of $(1.6–2.2) \times 10^{-4}$ mol (Figure 11(b)). Again, the threshold value of **N** at onset reads 1.298×10^{-4} mol, regardless of the presence or absence of the initial **H**. The results suggest that the slow accumulation of **N** via *M*2 reaching its threshold value is the rate-limiting step for hydrate onset. Only with sufficient accumulated **N** and **H** species could fast autocatalytic reactions (*M*4–*M*5) initiate rapid hydrate growth.

As Figure 12 shows, a pre-existing **H** did not result in immediate growth, but the **H** was consumed immediately to reach a pseudo-equilibrium before it accumulated gradually.

This could be related to the reaction kinetics. Before rapid growth (*M*4–*M*5) could occur, trace amounts of pre-existing **H** may have to be converted into **N** or dissociate into dissolved gas and water via the reverse process. This result may be attributed to and agree with the fact that the disintegration of hydrate clusters in a perturbing environment is more energetically favorable than its agglomeration.[46] This result suggests that the accumulation of oligomeric precursors and their conversion to hydrates are the determining steps in the overall hydrate nucleation and growth kinetics.

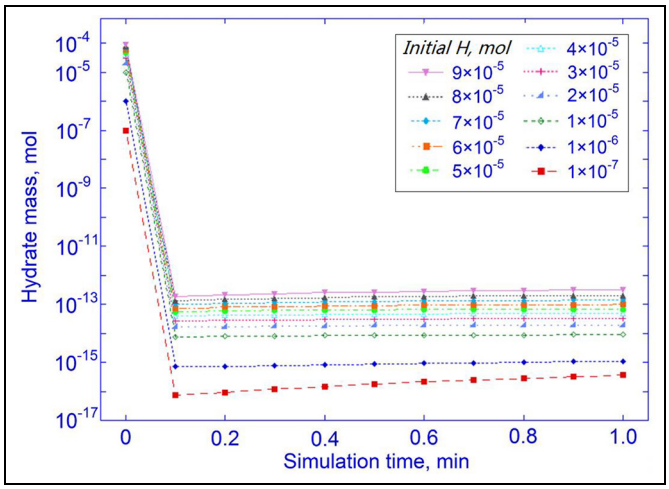

Figure 12. Hydrate mass variation in the first minute of simulation in the presence of pre-existing **H**.

Discussion

Gas solubility

The gas solubility will decrease upon the appearance of the solid hydrate phase, despite the decreased temperature in the hydrate region.[47,48] The rate constants k_1 and k_{-1} that were derived from gas-dissolution experiments are applicable to the induction stage only. With the hydrate onset that was observed in the reactor, or was simulated to occur, k_1 and k_{-1} may need to be re-evaluated for the post-nucleation stage. Rate constants k_1 and k_{-1} were approximated as constants in this work as it was difficult to determine the temperature-dependent solubility profile under the experimental PT with ongoing hydrate formation. This approximation will inevitably affect the accuracy of the simulation. With a reduced k_1 after hydrate onset, the simulated hydrate growth is expected to have a decreased growth rate as the growth stage proceeds with time. To improve the model, a more precise measurement of gas solubility as a kinetic variable in the presence of hydrate phase could be performed in future.

Particle concentration versus embryo size

According to classical nucleation theory,[49] nucleation is a dynamic process, and only hydrate nuclei that reach a critical size are energetically favorable to sustain growth. However, it is impractical to incorporate the embryo size as a valid parameter in the current reaction kinetics model. Instead, the modeling and simulation in this work concerns the hydrate-formation process from a mass/concentration perspective. An additional laser scanning module device mounted on the current experimental setup for real-time, in-situ monitoring and collection of particle information would help correlate the size and concentration of hydrate particles as a function of temperature, pressure, and properties of the reacting species. Such an updated system would allow observation of numerous simultaneously growing and shrinking crystal embryos, for experimental validation of our simulations with calculations of species concentrations. Future experimental reaction kinetics modeling and MD simulations are expected to provide new insights.

Memory effect and nucleation mechanism

The labile cluster hypothesis proposed by Sloan and co-workers[50,51] claims that hydrate nucleation starts with pure water. The essence is that the labile clusters formed from transient ring structures of water and dissolved gas eventually agglomerate into critical-sized nuclei and initiate subsequent growth. The memory effect says that one could expect faster nucleation if a hydrate-forming system is "seeded" with such labile clusters (equivalent to **N**) or hydrate nuclei (**H**). Our simulation shows that the hydrate-nucleation process was facilitated with a shortened induction if pre-existing **N** or **H** exceeded a certain level (1×10^{-5} mol for the current system). The simulation result supports the general claim of the memory effect that the presence of hydrate or any precursor structures in the aqueous phase could help trigger a faster hydrate onset.

The local structuring nucleation hypothesis that was proposed by Radhakrishnan and Trout[46] claims that nucleation starts with dissolved gas. They argue that the spatial configuration of dissolved gas molecules is rearranged first because of local thermal fluctuations which perturb the water structures around them. A recent MD study by Vatamanu and Kusalik[52] suggests that it is unnecessary for hydrate-like structures to remain or be "remembered" for faster nucleation. Instead, higher concentrations of dissolved gas are the promoting factor. However, simulations that we performed by assigning initially dissolved gas at time zero gave different results. The amounts of CH_4(aq) and C_3H_8(aq) in the simulation upon hydrate onset in a fresh system reach 8.7×10^{-4} and 7.0×10^{-5} mol, respectively. By assigning their initial amounts at time zero to these values, the numerical computations gave identical amounts of **N** and **H** at onset and the same growth rate thereafter. Only a slight decrease in simulated induction time was observed, where the change was insignificant (198.3 min vs 199.9 min). These results do not favor the local structuring nucleation hypothesis and the above MD simulation results. The role gas molecules play in hydrate nucleation should not be overemphasized.

The most recent "blob mechanism" for hydrate nucleation that was proposed by Jacobson et al.[53] proposes an important item worth noting as related to the established model in this work. The blob hypothesis suggests that blobs of gas molecules with surrounding water form in a reversible manner, and nucleate and dissolve repeatedly with thermal fluctuations. When they exceed a critical size, the blobs emerge as amorphous clathrate by sharing faces and locking the water molecules into the cages to cement the crystalline structure. Thereafter, the amorphous clathrate eventually evolves into stable hydrate nanocrystals. The transient blobs and amorphous clathrate structures are in a sense equivalent to hydrate precursors **N** in our simulation work. The blob mechanism that highlights the reversible reactions appears to be a favored hypothesis in terms of reaction kinetics. Nevertheless, neither the life span of blobs in solution, nor the role of blobs or amorphous clathrate in the memory effect phenomena were specified. We postulate with our simulations that the preservation of such immature structures at a threshold level is the major cause of facilitated nucleation.

Conclusion

A reaction kinetics model was established to simulate s-II methane–propane hydrate formation, and the simulation results were compared to experimental data. Simulations show that the slow accumulation of precursors and their conversion to hydrates dominates the length

of nucleation induction and triggers rapid autocatalytic reactions for sustainable hydrate growth.

Simulations also show that pre-existing precursors or hydrate particles above a certain level facilitate hydrate nucleation with a shortened induction, without affecting the growth stage. It is encouraging that the established model could be used to study hydrate-formation kinetics and provide insight into the memory effect phenomenon and hydrate-nucleation mechanism. Being a worthwhile attempt to approach hydrate formation kinetics with elementary reactions, the simulation accuracy can be further improved by integrating dynamic, time-dependent rate constants.

Acknowledgements

W.K. would like to thank Professor Peter Ruoff at the Centre for Organelle Research, University of Stavanger, Norway, for sharing his invaluable experience in reaction kinetics modeling, without which this work could not have been initiated or completed.

Declaration of conflicting interests

The author(s) declared no potential conflicts of interest with respect to the research, authorship, and/or publication of this article.

Funding

The author(s) disclosed receipt of the following financial support for the research, authorship, and/or publication of this article: This work was supported by China Postdoctoral Science Foundation funded project (Grant no.: 2017M620050) and the National Natural Science Foundation of China (grant no.: 21808122).

Supplemental material

Supplemental material for this article is available online.

References

1. Sloan ED Jr. *Nature* 2003; 426: 353–363.
2. Jeffrey GA. *Inclusion compounds*. London: Academic Press, 1984, p. 135.
3. Steed JW and Atwood JL. *Supramolecular chemistry*. Hoboken, NJ: Wiley, 2013.
4. Sloan ED, Koh C and Sum AK. *Natural gas hydrates in flow assurance*. New York: Gulf Professional Publishing, 2011.
5. Kvenvolden KA and Lorenson TD. The global occurrence of natural gas hydrate. In: Paull CK and Dillon WP (eds) *Natural gas hydrates: occurrence, distribution, and detection*. Washington, DC: American Geophysical Union, 2011.
6. Boswell R. *Science* 2003 325: 957–958.
7. Kennett J.P et al. *Am Geophysc Union* 2003; 83: 513–516.
8. Dickens GR. *Science* 2003; 299: 1017–1017.
9. Dashti H, Yew LZ and Lou X. *J Nat Gas Sci Eng* 2015; 23: 195–207.
10. House KZ, Schrag DP, Harvey CF, et al. *Proc Natl Acad Sci* 2006; 103: 12291–12295.
11. Babu P, Linga P, Kumar R, et al. *Energy* 2015; 85: 261–279.
12. Veluswamy HP, Kumar R and Linga P. *Appl Energy* 2014; 122: 112–132.
13. Kang KC, Linga P, Park K-N, et al. *Desalination*, 2014; 353: 84–90.

14. Hashemi S, Macchi A and Servio P. *Ind Eng Chem Res* 2007; 46: 5907–5912.
15. Skovborg P and Rasmussen P. *Chem Eng Sci* 1994; 49: 1131–1143.
16. Herri JM, Pic JS, Gruy F, et al. *AIChE J* 1999; 45: 590–602.
17. Turner DJ, Miller KT and Sloan ED. *Chem Eng Sci* 2009; 64: 3996–4004.
18. Uchida T, Ebinuma T, Kawabata J, et al. *J Cryst Growth* 1999; 204: 348–356.
19. Mori Y.H. *J Cryst Growth* 2001; 223: 206–212.
20. Mochizuki T and Mori YH. *J Cryst Growth* 2006; 290: 642–652.
21. Meindinyo R-ET, Svartaas TM, Nordbø TN, et al. *Energy Fuels* 2015; 29: 587–594.
22. Shindo Y, Lund PC, Fujioka Y, et al. *Energy Convers Manage* 1993; 34: 1073–1079.
23. Shindo Y, Lund PC, Fujioka Y, et al. *Int J Chem Kinet* 1993; 25: 777–782.
24. Lund PC, Shindo Y, Fujioka Y, et al. *Int J Chem Kinet* 1994; 26: 289–297.
25. Bollavaram P, Devarakonda S, Selim MS, et al. *Ann NY Acad Sci* 2000; 912: 533–543.
26. Freer EM, Selim MS and Sloan ED. *Fluid Phase Equilib* 2001; 185: 65–75.
27. Mu L, Li S, Ma Q-L, et al. *Fluid Phase Equilib* 2014; 362: 28–34.
28. Shi B-H, Gong J, Sun C-Y, et al. *Chem Eng J* 2011; 171: 1308–1316.
29. Vysniauskas A and Bishnoi PR. *Chem Eng Sci* 1983; 38: 1061–1072.
30. Vysniauskas A and Bishnoi PR. *Chem Eng Sci* 1985; 40: 299–303.
31. Lekvam K. and Ruoff P. *J Am Chem Soc* 1993; 115: 8565–8569.
32. Englezos P, Kalogerakis N, Dholabhai PD, et al. *Chem Eng Sci* 1987; 42: 2659–2666.
33. Englezos P, Kalogerakis N, Dholabhai PD, et al. *Chem Eng Sci* 1987; 42: 2647–2658.
34. Pilling MJ and Seakins PW. *Reaction kinetics*. 2nd ed. Oxford: Oxford University Press, 1996.
35. Israelachvili JN. *Intermolecular and surface forces*. 3rd ed. Amsterdam: Elsevier, 2011.
36. Parent JS and Bishnoi PR. *Chem Eng Commun* 1996; 144: 51–64.
37. Takeya S, Hori A, Hondoh T, et al. *J Phys Chem B* 2000; 104: 4164–4168.
38. Sloan ED, Subramanian S, Matthews PN, et al. *Ind Eng Chem Res* 1998; 37: 3124–3132.
39. Bylov M and Rasmussen P. *Chem Eng Sci* 1997; 52: 3295–3301.
40. Báez LA and Clancy P. *Ann NY Acad Sci* 1994; 715: 177–186.
41. Rodger PM. *Ann NY Acad Sci* 2000; 912: 474–482.
42. Yasuoka K and Murakoshi S. *Ann NY Acad Sci* 2000; 912: 678–684.
43. Abay HK and Svartaas TM. *Energ Fuel* 2011; 25: 42–51.
44. Hindmarsh AC. *ACM SIGNUM Newsletter* 1980; 15: 10–11.
45. Ohmura R, Ogawa M, Yasuoka K, et al. *J Phys Chem B* 2003; 107: 5289–5293.
46. Radhakrishnan R and Trout BL. *J Chem Phys* 2002; 117: 1786–1796.
47. Taylor CJ, Miller KT, Koh CA, et al. *Chem Eng Sci* 2007; 62: 6524–6533.
48. Handa YP. *J Phys Chem* 1990; 94: 2652–2657.
49. Mullin JW. Nucleation. In: Mullin JW (ed.) *Crystallization*. Oxford: Butterworth Heinemann, 2001, pp. 181–215.
50. Sloan ED and Fleyfel F. *AIChE J* 1991; 37: 1281–1292.
51. Christiansen RL and Sloan ED. *Ann NY Acad Sci* 1994; 715: 283–305.
52. Vatamanu J and Kusalik PG. *Phys Chem Chem Phys* 2010; 12: 15065–15072.
53. Jacobson LC, Hujo W and Molinero V. *J Am Chem Soc* 2010; 132: 11806–11811.